ACSNANO

www.acsnano.org

ARTICLE

Nonintrusion Monitoring of Droplet Motion State *via* Liquid–Solid Contact Electrification

Zixuan Song,[⊥] Xiaosong Zhang,[⊥] Zheng Wang,[⊥] Tao Ren, Wei Long,* Tinghai Cheng,* and Zhong Lin Wang*

Cite This: https://doi.org/10.1021/acsnano.1c08691

Read Online

ACCESS | Metrics & More | Article Recommendations | Supporting Information

ABSTRACT: Droplet motion state monitoring is important in microfluidic applications, such as biomedicine, drug delivery, and metal ion extraction. Here, a nonintrusion monitoring method of droplet motion state *via* liquid–solid contact electrification is proposed, and a triboelectric droplet motion state sensor (TDMSS) is fabricated. Droplet counting and droplet size monitoring can be realized by signal processing and information extracting of the voltage pulse. The experimental results show that the number of droplets increases linearly with the increase of liquid flow, and the linearity is 0.9854. Moreover, TDMSS can stably monitor the number of droplets in different motion states. In addition, the output pulse width is sensitive to droplet size, and the droplet length ranges from 3 to 13.5 mm. More importantly, TDMSS can realize the function of droplet counting and size monitoring of a conductive liquid and accurate droplet counting under different inclination angles and motion states. This work not only provides a nonintrusion method for droplet motion state monitoring but also makes a solid step for microfluidic sensing technology based on a triboelectric nanogenerator.

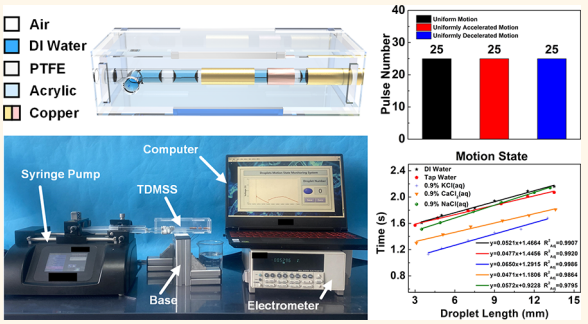

KEYWORDS: *liquid–solid contact electrification, nonintrusion monitoring, droplet counting, droplet size, motion state*

Droplet motion state monitoring is a great demand in the field of droplet microfluidics application.[1−3] The current droplet state monitoring technologies are mainly divided into intrusion monitoring and nonintrusion monitoring. Traditional intrusion monitoring usually uses a probe to measure the flow field in the tube, but it will cause interference to the flow field in the tube and affect the accuracy of the measurement.[4−7] Nonintrusion monitoring can avoid the influence of sensor components on the droplet motion state in the pipeline. Because of its high precision and strong intuition, it has been widely used and developed in recent years. It is mainly divided into optical sensing and electronic sensing. However, these two methods have the problems of complex equipment, high cost, and external power supply, which limit the application of nonintrusion monitoring sensors in complex environments.[8−11] Therefore, it is of great significance to propose a nonintrusion and self-powered monitoring method for droplet state monitoring in the tube.

The triboelectric nanogenerator (TENG) based on the coupling of contact electrification and electrostatic induction was invented by Prof. Wang and his team.[12] Due to its simple working mechanism and fabrication process, low cost, and efficient energy conversion, the TENG has been developed for micro/nano power sources,[13,14] self-powered sensing,[15−17] blue energy,[18−20] and high-voltage power sources.[21,22] Among them, the liquid–solid triboelectric nanogenerator has received extensive attention, and it has been used for motion sensors,[23,24] chemical sensors,[25−27] microfluidic actuators,[28,29] corrosion protection,[30,31] level gauges,[32−34] and so on.[35,36] For instance, Zhao *et al.* developed prototypes of a drainage bottle droplet sensor and a smart intravenous injection monitor based on the superhydrophobic liquid–solid contact TENG.[37] Ping *et al.* designed a triboelectric nanogenerator to collect raindrop energy in an agricultural environment, which realized the self-power supply of a greenhouse.[38] Thus, the self-powered sensing based on the liquid–solid contact electrification is feasible and stable.

In this paper, a nonintrusion monitoring method of droplet motion state is proposed. Based on liquid–solid contact electrification, a triboelectric droplet motion state sensor

Received: October 2, 2021
Accepted: October 19, 2021

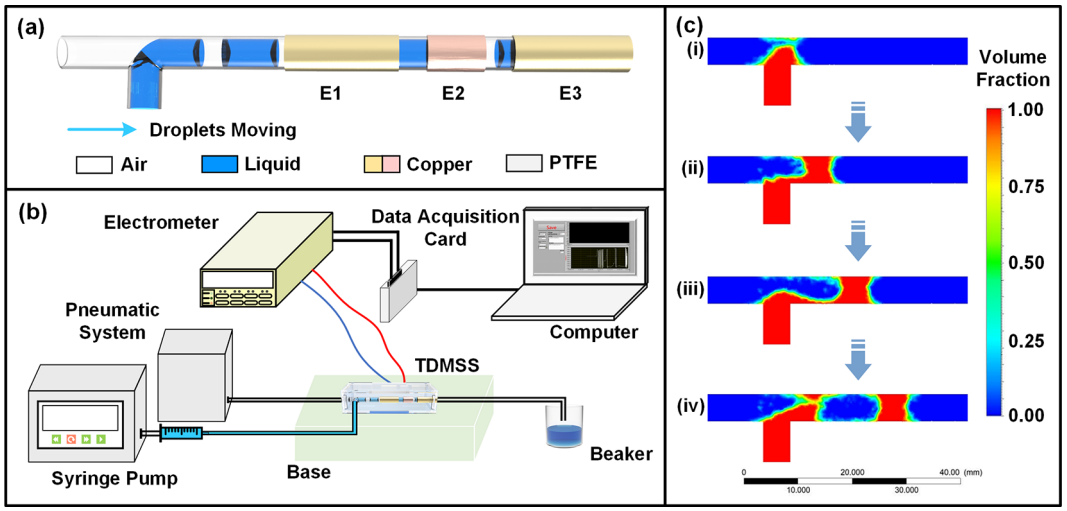

Figure 1. Structure of the droplet motion state triboelectric sensor (TDMSS) and simulation diagram of the flow field in the tube: (a) structure of the TDMSS, (b) schematic diagram of the testing setup, (c) flow field simulation of droplet generation in the tube.

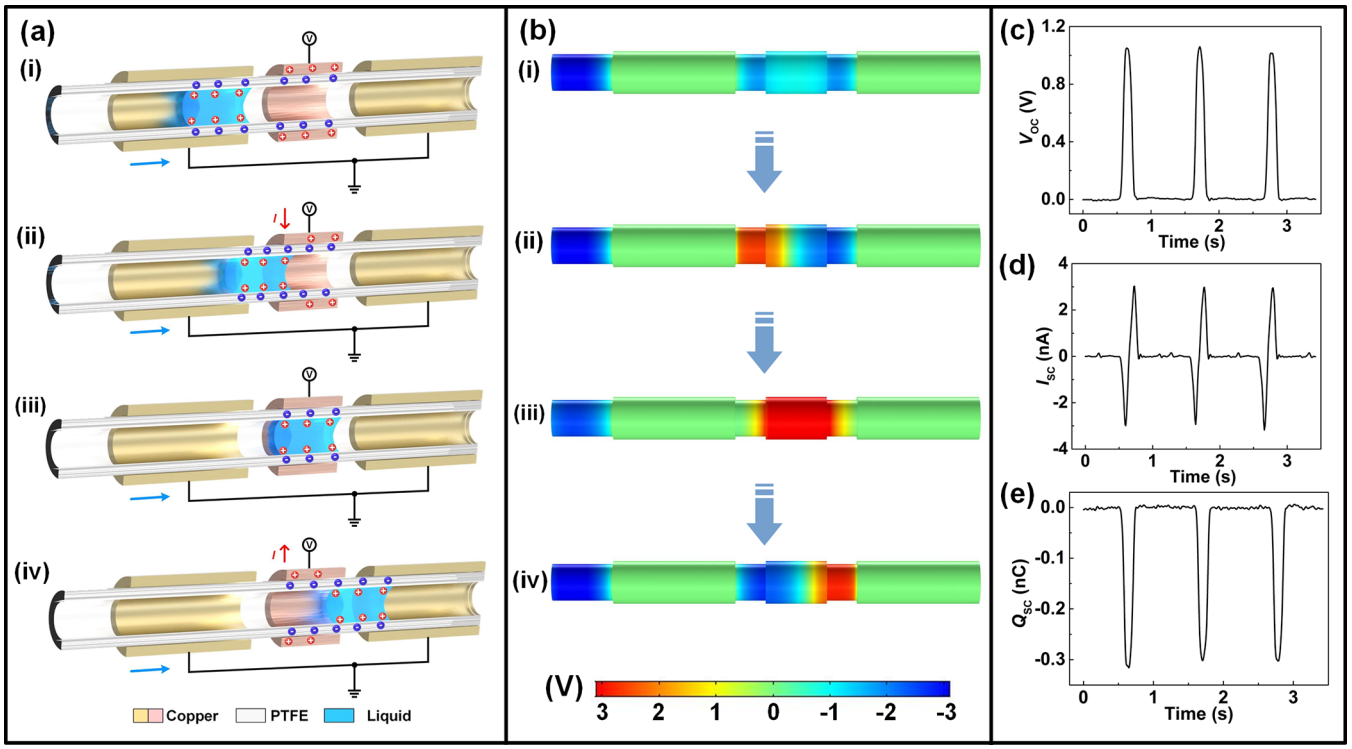

Figure 2. Working mechanism and basic performance test of the TDMSS: (a) schematic diagram of the working mechanism of the TDMSS, (b) COMSOL simulation of the potential distribution of droplets at four different positions in the TDMSS, (c–e) basic performance test of the TDMSS, including (c) open-circuit voltage, (d) short-circuit current, and (e) transfer charge.

(TDMSS) is fabricated. The TDMSS consists of a T-junction, a PTFE tube, and three copper electrodes. Special electrode arrangement of the TDMSS can effectively shield the signal interference caused by the contact between droplets and the PTFE tube. The experimental results show that the system can stably realize droplet counting because of the good linear relationship between the number of voltage pulses and liquid flow rate. Moreover, TDMSS shows the advantage of stable counting under different liquid mediums, inclination angles, and droplet motion states. In addition, droplets with a length of 3.0 to 13.5 mm can be successfully monitored by TDMSS, and the actual length of droplets has good linearity with the time they pass through the electrode. This work has broad application fields in the future, such as biomedical detection, pipeline transportation monitoring, and hydrometallurgy.

RESULTS AND DISCUSSION

Structure Design and Working Principle of the TDMSS. As illustrated in Figure 1a, the TDMSS is mainly assembled with a droplet formation part and a sensing unit. The droplet formation part is composed of a T-junction and a PTFE tube. The sensing part of the TDMSS is mainly monitored by the effective sensing region (E2). The electrodes (E1 and E3) distributed on both sides of E2 are grounded to

https://doi.org/10.1021/acsnano.1c08691
ACS Nano XXXX, XXX, XXX−XXX

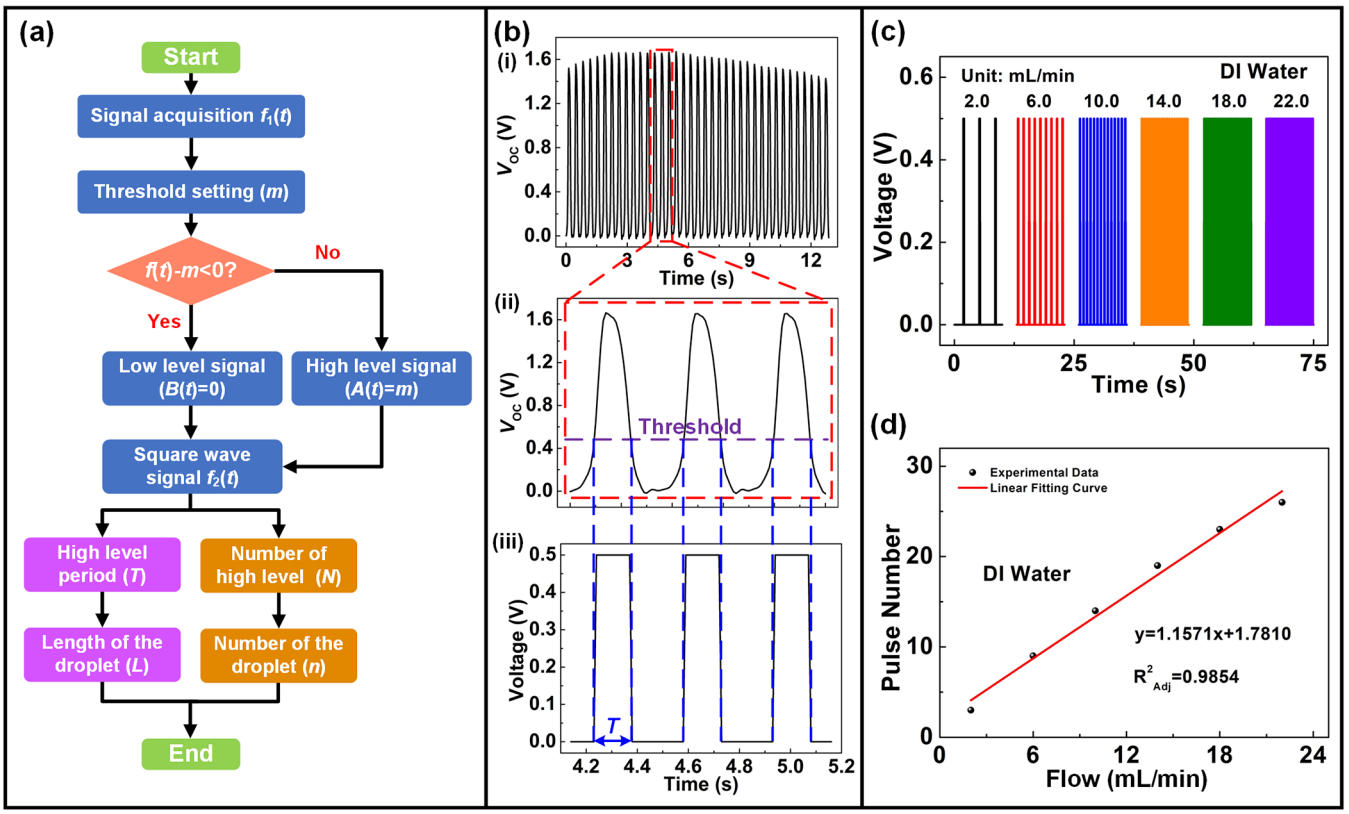

Figure 3. Performance of droplet counting monitoring under different flow rates: (a) flowchart of the droplet state monitoring program, (b) signal processing of the program includes (i) original data of open-circuit voltage, (ii) data extraction, and (iii) program processing, (c) voltage under different flow rates in the same time, (d) fitting diagram of voltage pulse number and flow rate.

shield the signal interference caused by the contact between the droplets and the PTFE tube. The electrode arrangement optimizes the traditional single-electrode mode. When the droplet contacts the tube, liquid–solid contact electrification makes electrons flow on the PTFE surface and flow into the ground along the grounding electrodes. Therefore, the electrode arrangement can shield the additional charge generated by the contact between the PTFE tube and droplets. Figure 1b shows a schematic diagram of a complete droplet motion state monitoring platform. The air provided by the pneumatic system plays two roles in the system. One is to shear the liquid to generate droplets. The other is to drive droplets to flow in the tube as one of the driving forces, and the gas almost does not provide additional charges for the droplet. When droplets pass through E2, corresponding electrical signals will be generated and monitored through an electrometer and a data acquisition card. Finally, the droplet information is displayed on the computer.

According to the actual size and working conditions of the TDMSS, the flow field of droplets generated in the PTFE tube is numerically simulated (Figure 1c). The discrete and independent droplets are produced by the combined action of the shear force of air on water and the extrusion force on the inner wall of the tube. By adjusting the gas flow of the pneumatic system and the liquid flow of the syringe pump, respectively, droplets with different generation frequencies and sizes can be generated (Note S1, Supporting Information).

Figure 2 shows the working mechanism of the TDMSS, the numerical simulation of the potential distribution of droplets in the pipeline, and its basic performance curve. Figure 2a shows the contact process between droplets and PTFE caused by contact electrification, which is helpful to better understand the main performance curve shown in Figure 2c. A PTFE tube is used as a solid friction layer due to its high electronegativity, while liquid is selected as another friction material.

When the droplets enter the PTFE tube, the triboelectric effect will cause the droplets to produce a net positive charge, and the surface of the PTFE tube has an evenly distributed net negative charge. At this time, a positive charge is distributed on the E2 surface. When the droplet and E1 completely overlap [Figure 2a(i)], the charge generated by the contact between the droplet and the tube flows into the ground along the wire due to the grounding of E1 and E3. Therefore, it is in static equilibrium at this position. When the overlapping area between the droplet and E2 gradually increases [Figure 2a(ii)], the surface charge begins to separate, and the electrostatic balance between the droplet and E1 is broken. The resulting voltage value gradually increases. And the Earth supplies positive charges to E2. If the charge in the direction from the electrode into the Earth is positive, the short-circuit current direction is opposite of the positive direction, so a negative peak current is displayed. Next, when the droplet moves to a position completely coincident with E2 [Figure 2a(iii)], it is in a second electrostatic equilibrium state without electron transfer. The open-circuit voltage reaches the maximum and the short-circuit current is 0. Finally, when the droplet leaves E2 [Figure 2a(iv)], the potential difference is generated again, and the voltage decreases with the decrease of the overlapping area between the droplet and E2. At this time, the positive charge on E2 flows into the Earth, which is consistent with the positive direction, so the short-circuit current is positive. E2 and the PTFE tube realize electrostatic

https://doi.org/10.1021/acsnano.1c08691
ACS Nano XXXX, XXX, XXX–XXX

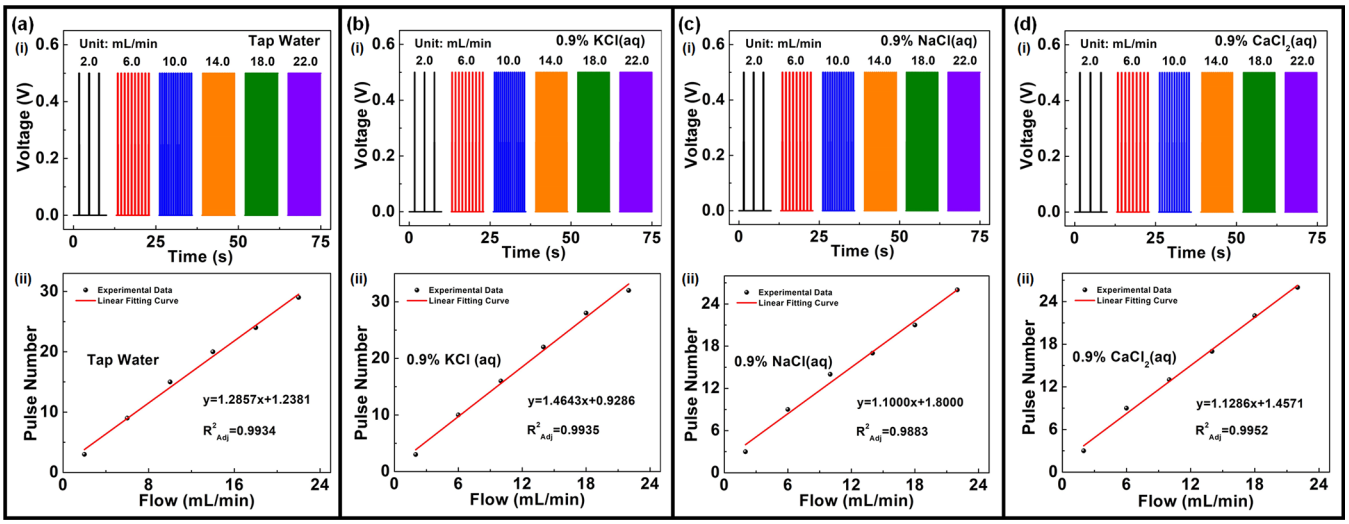

Figure 4. Performance of droplet counting monitoring under different liquid mediums: (a) tap water, (b) 0.9% KCl(aq), (c) 0.9% NaCl(aq), (d) 0.9% $CaCl_2$(aq).

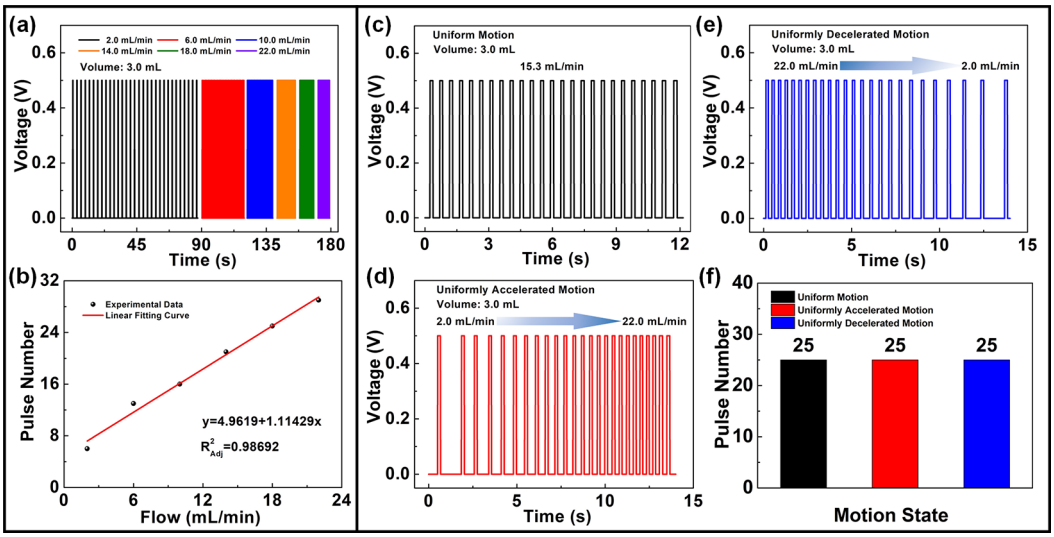

Figure 5. Performance of droplet counting monitoring under different motion states: (a) open-circuit voltage of droplets at different flows in uniform motion, (b) linear relationship between flow rates and the number of pulses in uniform motion, (c) output voltage in uniform motion, (d) output voltage in uniformly accelerated motion, (e) output voltage in uniformly decelerated motion, (f) number of pulses in different motion states.

balance again when the droplet completely leaves E2. The transfer charge curve is consistent with the open-circuit voltage curve. Therefore, the droplet completes a complete performance curve cycle.

To more intuitively understand the working mechanism of the TDMSS, COMSOL Multiphysics 5.5 is used to simulate the potential distribution of droplets at four positions in the PTFE tube (Figure 2b). The simulation results are consistent with the above analysis, which proves the feasibility of the principle. Figure 2c–e show the basic output performance of the three droplets monitored by the TDMSS, including open-circuit voltage (Figure 2c), short-circuit current (Figure 2d), and transfer charge (Figure 2e). It can be seen that the performance test curve of the TDMSS is consistent with the above principle analysis results, which verifies the feasibility of the TDMSS principle.

Performance of the TDMSS. The flowchart of signal processing by the droplet motion state monitoring program is shown in Figure 3a. The program is processed and analyzed in MATLAB. By judging the difference between the original signal and the threshold value, the trend of the triboelectric signal is analyzed. When the original signal is less than the threshold, the program determines that the voltage amplitude of the signal is 0. On the contrary, the voltage amplitude is the threshold at this time. Figure 3b shows the process of processing data with the program. First, part of the signal [Figure 3b(ii)] is extracted from the original signal [Figure 3b(i)], and a threshold value is set in the program. When the signal rises or falls in the threshold value, an edge jump occurs, from which a square wave signal is obtained [Figure 3b(iii)]. The pulse number and pulse width can be directly determined by the signal processed by the program. According to the basic output voltage value, 0.5 V as the program threshold for subsequent experiments was selected.

To verify the droplet counting performance of the sensor, the output voltage processed by the program at different flow

https://doi.org/10.1021/acsnano.1c08691
ACS Nano XXXX, XXX, XXX−XXX

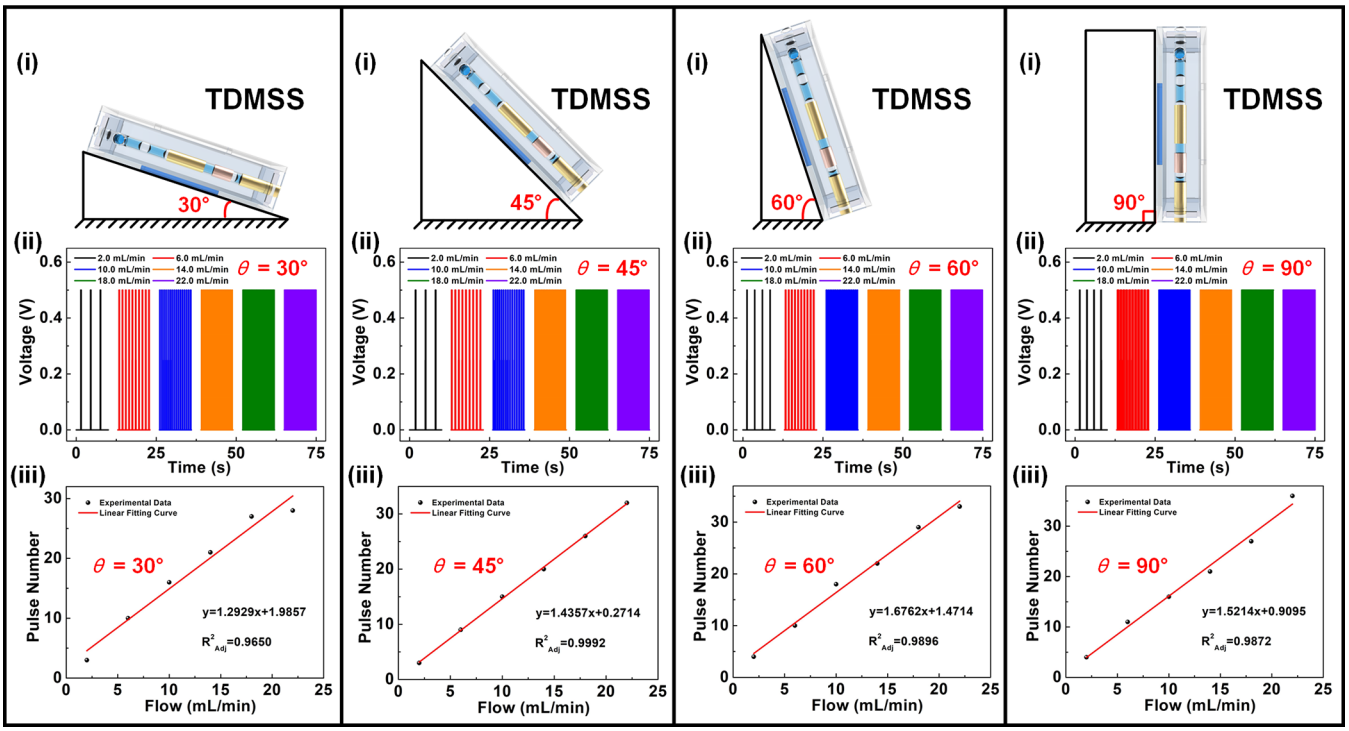

Figure 6. Performance of the TDMSS in monitoring the number of DI water droplets under different inclination angles: (a) $\theta = 30°$; (b) $\theta = 45°$; (c) $\theta = 60°$; (d) $\theta = 90°$.

rates in equal time is shown in Figure 3c. The original signal measured is shown in Figure S1a. The flow measurement range is 2 to 22 mL/min, and the flow rate increases by 4 mL/min in each step. The experimental results indicate that the pulse number is proportional to the flow rate. Accordingly, the frequency of droplet generation is directly proportional to the flow rate. Besides, Figure 3d shows that there is a good linear relationship between the number of output voltage pulses and the liquid flow rate of the syringe pump, and the linearity is 0.9854. This shows that the droplet counting function of the TDMSS has good stability.

As one of the application fields of the TDMSS is biomedicine, the concentration of stroke-physiological saline solution is taken as a reference. Some common conductive liquids are selected for the droplet counting performance test, such as 0.9% KCl(aq), 0.9% NaCl(aq), and 0.9% $CaCl_2$(aq). Figure 4 shows the droplet counting performance of different liquid mediums. The original data of the voltage are shown in Figure S1(b)−(e). The experimental results show that the counting performance of the TDMSS is not affected by the change of liquid medium, and the number of droplets produced by different mediums can still be stably monitored. In addition, there are some differences in the number of droplets per liquid. This is because different liquids have different physical properties such as density, viscosity, and surface tension, which may affect the formation of droplets. According to the number of droplets monitored by TDMSS, it shows a good linear relationship between liquid flow rate and the number of pulses, and their linearities are 0.9934, 0.9935, 0.9883, and 0.9952, respectively. This proves that the conductive liquid can also be applied to the droplet counting of the TDMSS.

Figure 5 shows the monitoring of droplet counting in 3 mL of DI water in different motion states. Figure 5a shows the voltage performance of droplets produced at different flow rates in uniform motion, and the original signal obtained from the experiment is shown in Figure S2. The number of droplets produced by 3 mL of DI water decreases with the increase of flow rate. This is because the droplet size is inversely proportional to the liquid flow when the gas flow is constant. Moreover, the flow rate of DI water has a good linear relationship with the output pulse number, and the linearity is 0.9517 (Figure 5b).

According to the droplet formation mechanism, the formation of droplets is determined by the combined action of the shear force of air on the liquid and the extrusion force of the inner wall of the tube against the liquid. The flow of droplets in the tube is determined by the gas phase and liquid phase. Therefore, when the gas phase flow rate remains constant, the liquid flow rate accelerated or decelerated uniformly, which will directly affect the motion state of droplets in the tube. According to the output voltage signal of the TDMSS, the motion state of droplets in the tube can be qualitatively judged, such as uniform motion, uniformly accelerated motion, and uniformly decelerated motion (Figure 5c−e). The time interval between droplets is the same (Figure 5c). That is, the motion state of droplets in the tube is uniform motion. Figure 5d shows that the TDMSS detects that the droplets flow through the PTFE tube in a uniformly accelerated motion state. Similarly, the droplets moving through the PTFE tube uniformly decelerated can still be monitored by the TDMSS. The original data of droplets in different motion states are shown in Figure S2. The number of droplets uniformly accelerated and uniformly decelerated is monitored by the TDMSS. The flow rate of uniform motion is calculated according to the linear formula in Figure 5b and then verified by experiments (Figure 5f). The experimental results show that the droplet number of uniform motion is

https://doi.org/10.1021/acsnano.1c08691
ACS Nano XXXX, XXX, XXX−XXX

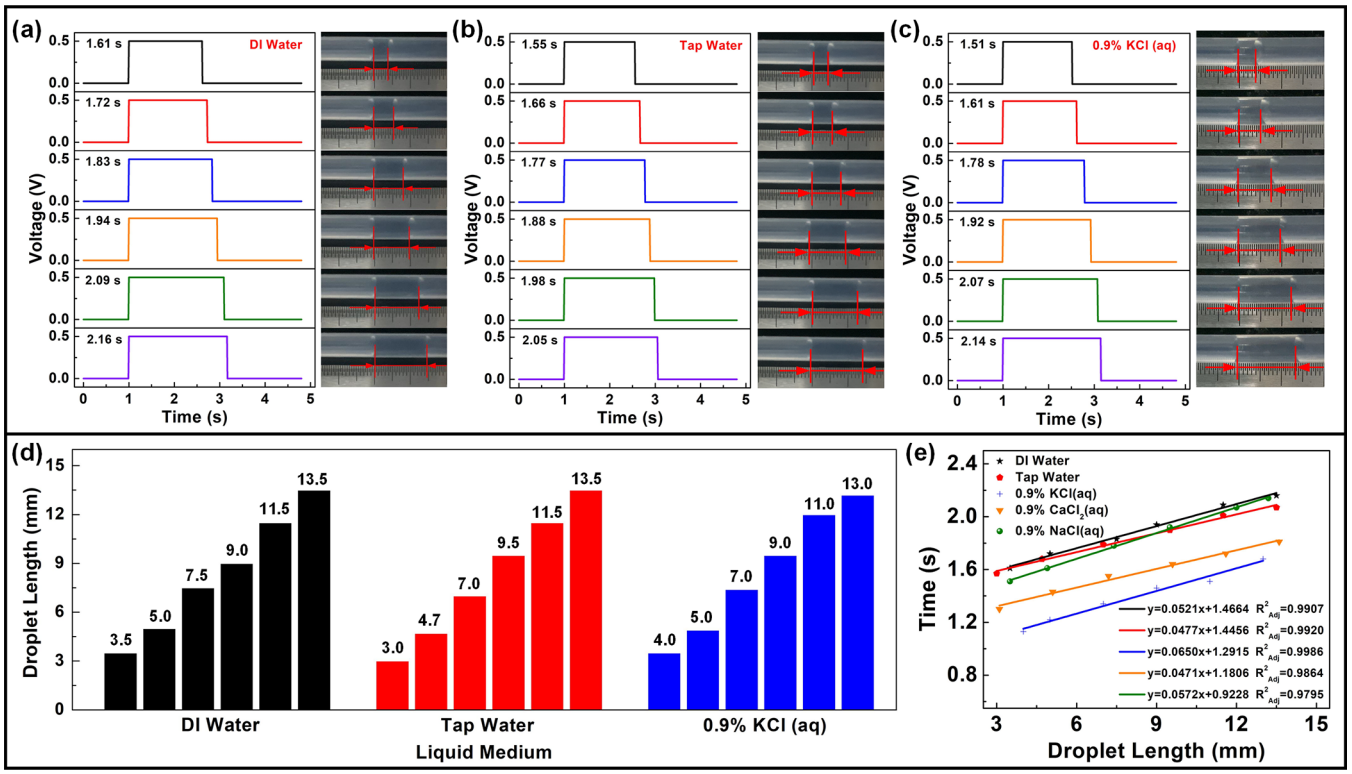

Figure 7. Performance of droplet size monitoring under different mediums: (a) experimental photos of droplets in three liquid mediums and voltage pulse curves of droplets passing through an electrode, (b) actual sizes of droplets in the experiment, (c) linear relationships between the length of different droplets and the time passing through the electrode.

consistent with that of the other two kinds of variable motion. This not only verifies the accuracy of the linear formula but also proves that the TDMSS can monitor the counting ability under different motion states.

The above TDMSS counting performance experiments are carried out under horizontal conditions. To test the counting performance of the TDMSS under different angles, the TDMSS is fixed on the inclined planes with different angles (Figure 6a–d). The experiments of DI water with inclination angles of 30°, 45°, 60°, and 90° at flow rates of 2 to 22 mL/min are carried out. Experimental results show that changing the inclination angle does not affect the counting performance of the TDMSS. On the oblique plane from 30° to 90°, the TDMSS can still stably monitor the number of DI water droplets. The original data of open-circuit voltage and the number of droplets are shown in Figure S3. When the TDMSS is placed at a certain angle, the liquid in the tube is not only affected by the shear force of air on the tube and the extrusion on the inner wall but also affected by gravity. Under the influence of gravity, the liquid may be more easily cut by air to form droplets. Therefore, the number of droplets varies slightly at different angles. In addition, there is a good linear relationship between the liquid flow and the number of voltage pulses under four angles, and the linearity is 0.9650, 09992, 0.9896, and 0.9872, respectively. At the same time, it also proves that the TDMSS can still count normally under different angles.

The performance of droplet size monitoring by the TDMSS is shown in Figure 7. Keeping the gas flow rate constant and changing the liquid flow rate produces different lengths of droplets. DI water and common conductive liquids [tap water and 0.9% KCl(aq)] are selected for the droplet size monitoring experiment. Figure 7a–c show the experimental photos of droplets in three different mediums at different sizes and the voltage pulse signal curve generated by droplets passing through the E2. The pulse width is defined as the time required for the droplet to pass through E2. It can be seen from the experimental photos that the droplets in the PTFE tube are concave at both ends, which is determined by the physical properties of the liquid, and the key factor is surface tension. The surface tension of the liquid is small; that is, the tension between the liquid and liquid molecules is less than that between the liquid and the PTFE tube's inner wall. Therefore, a concave liquid surface is formed at the interface between the liquid and the PTFE. Considering this phenomenon, the distance between the lowest point of the concave surface at both ends of the droplet is taken as the actual length.

Figure 7d shows the actual size of the droplets generated by three mediums in the experiment, between 3 and 13.5 mm. Different droplet sizes under different mediums are normal. Due to the different physical properties of the liquid itself, the formation of droplets may be affected. The experimental results show that the size monitoring of DI water, tap water, and 0.9% KCl(aq) has good linearities, which are 0.9907, 0.9920, and 0.9986, respectively. Further, two other conductive liquids [0.9% NaCl(aq) and 0.9% $CaCl_2$(aq)] are selected for size monitoring experiments and also obtain good linear relationships (Figure 7e). The TDMSS monitors the original data of the droplet size output signal of five kinds of liquid, and the experimental photos of 0.9% NaCl(aq) droplets and 0.9% $CaCl_2$(aq) droplets are shown in Figure S4. This proves that TDMSS size monitoring is also applicable to DI water and conductive liquids and provides a monitoring method for pipeline transportation in industrial fields.

https://doi.org/10.1021/acsnano.1c08691
ACS Nano XXXX, XXX, XXX–XXX

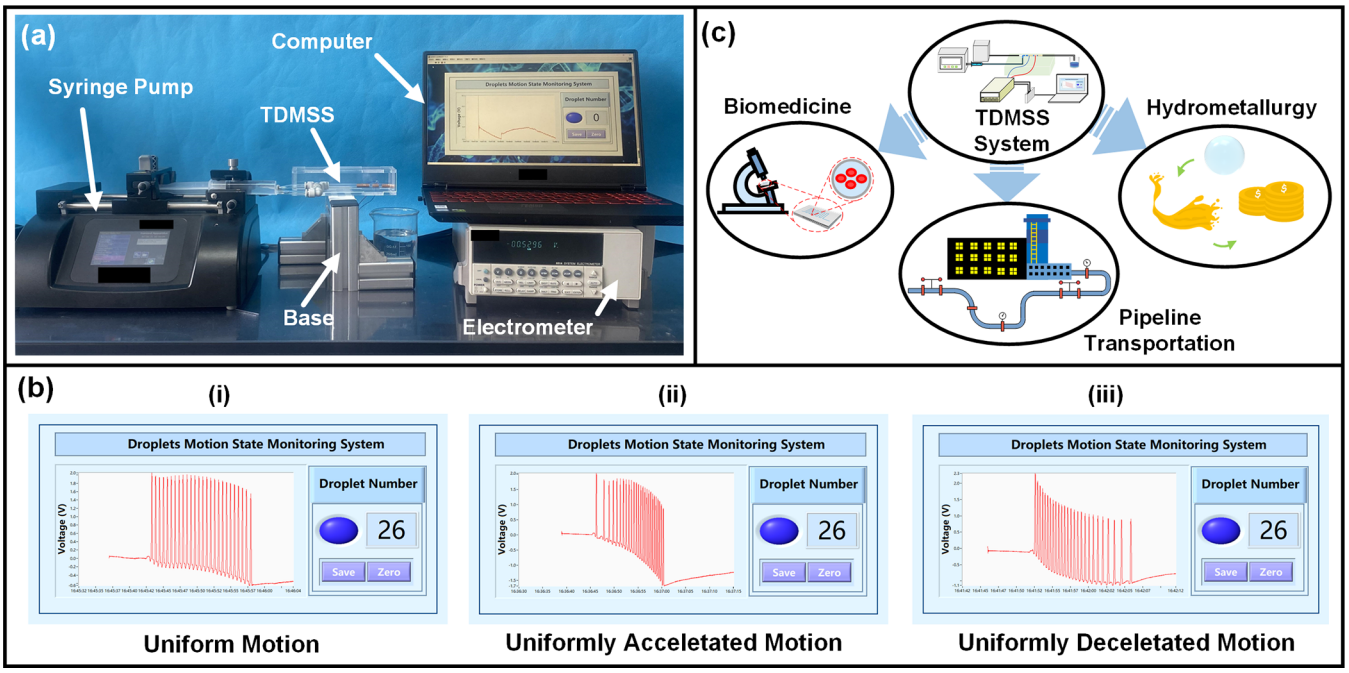

Figure 8. LabVIEW interface display and application prospects of the TDMSS: (a) actual monitoring system of the TDMSS, (b) interface display of droplet monitors under different motion states, (c) application prospects of the TDMSS in various scenarios.

Demonstration of the TDMSS. The droplet motion state monitoring system and its application prospects are shown in Figure 8. A demonstration of droplet counting using the TDMSS is given in Video S1 in the Supporting Information.

Figure 8a shows the TDMSS monitoring system. The TDMSS is placed in an acrylic box to reduce the impact of the external environment, such as air humidity and environmental interference. The two inlets of the TDMSS are connected to the liquid and gas input systems, respectively. The syringe pump and throttle valve are used to accurately control the flow rate of the liquid and gas. The original output voltage monitored by the TDMSS is displayed through the LabVIEW interface, and the pulses are counted in the meanwhile. Figure 8b shows that the TDMSS is used to monitor the original output voltage and the number of droplets of the same volume of DI water under different motion states within the flow range of 2 to 22 mL/min. The number of droplets produced by uniform motion, uniformly accelerated motion, and uniformly decelerated motion are 26, respectively. It is proved that the TDMSS monitoring system has excellent stability and responsiveness. Figure 8c shows that the TDMSS experimental system has broad application fields in the future, such as biomedical detection, pipeline transportation monitoring, and hydrometallurgy.

CONCLUSIONS

In summary, a nonintrusion monitoring method for droplet motion state *via* liquid−solid contact electrification was proposed, and a triboelectric droplet motion state sensor was fabricated. The corresponding pulse signal was generated when droplets passed through the PTFE tube with a special electrode arrangement. Droplet counting and droplet size can be monitored by processing signals and extracting information. Experimental results show that the system can stably realize droplet counting since the output voltage pulse number is linearly related to the liquid input flow. TDMSS can also realize normal counting and size monitoring under different environmental conditions, such as liquid medium and inclination angles. It is proved that the TDMSS has good stability and responsiveness. In addition, the output pulse width of TDMSS has good sensitivity to the droplet size, and the droplet length ranges from 3.0 to 13.5 mm. The size monitoring function is also applicable to conductive liquids. The nonintrusion monitoring method can provide reference and guidance for biomedicine, pipeline transportation monitoring, and hydrometallurgy.

EXPERIMENTAL SECTION

Fabrication of the TDMSS. The triboelectric droplet motion state sensor is composed of a shell part, a droplet generation part, and a monitoring sensing unit. The shell is a cubic shell assembled from an acrylic plate that is 160 mm long, 50 mm wide, and 40 mm high. The droplet generation part consists of a T-junction and a PTFE tube. The inner diameters of the T-junction are all 6 mm, and the PTFE tube is 5 mm in inner diameter, 6 mm in outer diameter, and 120 mm in length. The monitoring and sensing unit of the TDMSS is mainly composed of three copper electrodes (E1, E2, and E3). E2 is the main electrode; E1 and E3 are distributed on both sides of E1. As shown in Figure 1a, E1 is a copper electrode with a width of 10 mm attached 35 mm away from the outlet of the PTFE tube. The other two copper electrodes distributed on both sides of E2 are E1 and E3, with a width of 20 mm, respectively. Furthermore, the distances between them and E1 are 5 mm.

Measurement of the TDMSS. An electrometer (model 6514, Keithley) and a data acquisition card (NI USB-6211) are used to measure the output performance of the TDMSS. To measure the output performance of the TDMSS under different flows, the syringe pump (PHD ULTRA, Harvard USA) is used to control the flow of the liquid. A pressure-regulating valve (IR3020-04) and a throttle valve (AS3002F-08, SMC Japan) are used to control the pressure and flow of the pneumatic system. In the experiment, the pressure is always 0.05 MPa.

https://doi.org/10.1021/acsnano.1c08691
ACS Nano XXXX, XXX, XXX−XXX

ASSOCIATED CONTENT

Supporting Information

The Supporting Information is available free of charge at https://pubs.acs.org/doi/10.1021/acsnano.1c08691.

Original signal of droplet counting under different liquid mediums; original signal of open-circuit voltage of droplets under different motions; original signal of the TDMSS in DI water droplet counting under different inclination angles; original data of output voltage generated by droplets under different liquid mediums, and experimental photos of some droplets; principle and specific method of droplet generation in the T-junction (PDF)

Supporting Video S1: Demonstration of the TDMSS in droplet motion state monitoring (MP4)

AUTHOR INFORMATION

Corresponding Authors

Wei Long − *Faculty of Mechanical and Electrical Engineering, Kunming University of Science and Technology, Kunming, Yunnan 650550, China*; Email: daifor@163.com

Tinghai Cheng − *Beijing Institute of Nanoenergy and Nanosystems, Chinese Academy of Sciences, Beijing 101400, China; CUSTech Institute of Technology, Wenzhou, Zhejiang 325024, China*; orcid.org/0000-0003-0335-7614; Email: chengtinghai@binn.cas.cn

Zhong Lin Wang − *Beijing Institute of Nanoenergy and Nanosystems, Chinese Academy of Sciences, Beijing 101400, China; CUSTech Institute of Technology, Wenzhou, Zhejiang 325024, China; School of Materials Science and Engineering, Georgia Institute of Technology, Atlanta, Georgia 30332-0245, United States*; orcid.org/0000-0002-5530-0380; Email: zhong.wang@mse.gatech.edu

Authors

Zixuan Song − *Beijing Institute of Nanoenergy and Nanosystems, Chinese Academy of Sciences, Beijing 101400, China; Faculty of Mechanical and Electrical Engineering, Kunming University of Science and Technology, Kunming, Yunnan 650550, China*

Xiaosong Zhang − *Beijing Institute of Nanoenergy and Nanosystems, Chinese Academy of Sciences, Beijing 101400, China*

Zheng Wang − *Beijing Institute of Nanoenergy and Nanosystems, Chinese Academy of Sciences, Beijing 101400, China*

Tao Ren − *Faculty of Mechanical and Electrical Engineering, Kunming University of Science and Technology, Kunming, Yunnan 650550, China*

Complete contact information is available at: https://pubs.acs.org/10.1021/acsnano.1c08691

Author Contributions

⊥Z.S., X.Z., and Z.W. contributed equally to this work.

Notes

The authors declare no competing financial interest.

ACKNOWLEDGMENTS

The authors are grateful for the support received from the National Key R&D Project from the Minister of Science and Technology (Nos. 2016YFA0202701 and 2016YFA0202704), the Beijing Municipal Science and Technology Commission (No. Z171100002017017), and Yunnan Province Ten-thousand Talents Program/Youth Top-notch Talent Program (No. YNWR-QNBJ-2018-162).

REFERENCES

(1) Garstecki, P.; Fuerstman, M. J.; Stone, H. A.; Whitesides, G. M. Formation of Droplets and Bubbles in a Microfluidic T-Junction-Scaling and Mechanism of Break-Up. *Lab Chip* **2006**, *6*, 437−446.

(2) Logtenberg, H.; Lopez-Martinez, M. J.; Feringa, B. L.; Browne, W. R.; Verpoorte, E. Multiple Flow Profiles for Two-Phase Flow in Single Microfluidic Channels through Site-Selective Channel Coating. *Lab Chip* **2011**, *11*, 2030−2034.

(3) Doufene, K.; Tourne-Peteilh, C.; Etienne, P.; Aubert-Pouessel, A. Microfluidic Systems for Droplet Generation in Aqueous Continuous Phases: A Focus Review. *Langmuir* **2019**, *35*, 12597−12612.

(4) Dehkordi, P.; Colombo, L.; Mohammadian, E.; Arnone, D.; Azdarpour, A.; Sotgia, G. Study of Viscous Oil-Water-Gas Slug Flow in a Horizontal Pipe. *J. Pet. Sci. Eng.* **2019**, *178*, 1−13.

(5) Han, Y.; Jin, N.; Ren, Y.; Han, T.; Huang, Z. Measurement of Local Oil Holdup for Oil-in-Water Emulsion Flows Using Multiple Mini-Conductance Probes. *Measurement* **2018**, *121*, 6−18.

(6) Yang, Q.; Jin, N.; Wang, F.; Ren, W. Measurement of Gas Phase Distribution Using Multifiber Optical Probes in a Two-Phase Flow. *IEEE Sens. J.* **2020**, *20*, 6642−6651.

(7) Zhai, L.; Zhang, H.; Yan, C.; Jin, N. Measurement of Oil-Water Interface Characteristics in Horizontal Pipe Using a Conductance Parallel-Wire Array. *IEEE Trans. Instrum. Meas.* **2019**, *68*, 3232−3243.

(8) Nguyen, N.; Lassemono, S.; Chollet, F. Optical Detection for Droplet Size Control in Microfluidic Droplet-Based Analysis Systems. *Sens. Actuators, B* **2006**, *117*, 431−436.

(9) Elbuken, C.; Glawdel, T.; Chan, D.; Ren, C. Detection of Microdroplet Size and Speed Using Capacitive Sensors. *Sens. Actuators, A* **2011**, *171*, 55−62.

(10) Isgor, P. K.; Marcali, M.; Keser, M.; Elbuken, C. Microfluidic Droplet Content Detection Using Integrated Capacitive Sensors. *Sens. Actuators, B* **2015**, *210*, 669−675.

(11) Vincent, M.; Cassagnère, S.; Plantard, J.; Delville, J. Real-Time Droplet Caliper for Digital Microfluidics. *Microfluid. Nanofluid.* **2012**, *13*, 261−271.

(12) Fan, F.; Tian, Z.; Wang, Z. L. Flexible Triboelectric Generator. *Nano Energy* **2012**, *1*, 328−334.

(13) Wang, J.; Li, Y.; Xie, Z.; Xu, Y.; Zhou, J.; Cheng, T.; Zhao, H. i.; Wang, Z. L. Cylindrical Direct-Current Triboelectric Nanogenerator with Constant Output Current. *Adv. Energy Mater.* **2020**, *10*, 1904227.

(14) Wang, Y.; Yu, X.; Yin, M.; Wang, J.; Gao, Q.; Yu, Y.; Cheng, T.; Wang, Z. L. Gravity Triboelectric Nanogenerator for the Steady Harvesting of Natural Wind Energy. *Nano Energy* **2021**, *82*, 105740.

(15) Wang, Z.; Gao, Q.; Wang, Y.; Wang, J.; Wang, Y.; Cheng, T.; Wang, Z. L. Triboelectric Flow Sensor with Float-Cone Structure for Industrial Pneumatic System Monitoring. *Adv. Mater. Technol.* **2019**, *4*, 1900704.

(16) Xie, Z.; Dong, J.; Li, Y.; Gu, L.; Song, B.; Cheng, T.; Wang, Z. L. Triboelectric Rotational Speed Sensor Integrated into a Bearing: A Solid Step to Industrial Application. *Extreme Mech. Lett.* **2020**, *34*, 100595.

(17) Zhang, X.; Gao, Q.; Gao, Q.; Yu, X.; Cheng, T.; Wang, Z. L. Triboelectric Rotary Motion Sensor for Industrial-Grade Speed and Angle Monitoring. *Sensors* **2021**, *21*, 1713.

(18) Wang, Z. L.; Jiang, T.; Xu, L. Toward the Blue Energy Dream by Triboelectric Nanogenerator Networks. *Nano Energy* **2017**, *39*, 9−23.

(19) Zhang, C.; Liu, L.; Zhou, L.; Yin, X.; Wei, X.; Hu, Y.; Liu, Y.; Chen, S.; Wang, J.; Wang, Z. L. Self-Powered Sensor for Quantifying Ocean Surface Water Waves Based on Triboelectric Nanogenerator. *ACS Nano* **2020**, *14*, 7092−7100.

(20) Gu, H.; Zhang, N.; Zhou, Z.; Ye, S.; Wang, W.; Xu, W.; Zheng, H.; Song, Y.; Jiao, J.; Wang, Z.; Zhou, X. A Bulk Effect Liquid-Solid Generator with 3D Electrodes for Wave Energy Harvesting. *Nano Energy* **2021**, *87*, 106218.
(21) Liu, F.; Liu, Y.; Lu, Y.; Wang, Z.; Shi, Y.; Ji, L.; Cheng, J. Electrical Analysis of Triboelectric Nanogenerator for High Voltage Applications Exampled by DBD Microplasma. *Nano Energy* **2019**, *56*, 482−493.
(22) Lei, R.; Shi, Y.; Ding, Y.; Nie, J.; Li, S.; Wang, F.; Zhai, H.; Chen, X.; Wang, Z. L. Sustainable High-Voltage Source Based on Triboelectric Nanogenerator with a Charge Accumulation Strategy. *Energy Environ. Sci.* **2020**, *13*, 2178−2190.
(23) Shi, Q.; Wang, H.; Wang, T.; Lee, C. Self-Powered Liquid Triboelectric Microfluidic Sensor for Pressure Sensing and Finger Motion Monitoring Applications. *Nano Energy* **2016**, *30*, 450−459.
(24) Xu, M.; Wang, S.; Zhang, S.; Ding, W.; Kien, P.; Wang, C.; Li, Z.; Pan, X.; Wang, Z. L. A Highly-Sensitive Wave Sensor Based on Liquid-Solid Interfacing Triboelectric Nanogenerator for Smart Marine Equipment. *Nano Energy* **2019**, *57*, 574−580.
(25) Li, X.; Yeh, M.; Lin, Z.; Guo, H.; Yang, P.; Wang, J.; Wang, S.; Yu, R.; Zhang, T.; Wang, Z. L. Self-Powered Triboelectric Nanosensor for Microfluidics and Cavity Confined Solution Chemistry. *ACS Nano* **2015**, *9*, 11056−11063.
(26) Chen, B.; Tang, W.; He, C.; Jiang, T.; Xu, L.; Zhu, L.; Gu, G.; Chen, J.; Shao, J.; Luo, J.; Wang, Z. L. Ultrafine Capillary-Tube Triboelectric Nanogenerator as Active Sensor for Microliquid Biological and Chemical Sensing. *Adv. Mater. Technol.* **2018**, *3*, 1700229.
(27) Jiang, P.; Zhang, L.; Guo, H.; Chen, C.; Wu, C.; Zhang, S.; Wang, Z. L. Signal Output of Triboelectric Nanogenerator at Oil-Water-Solid Multiphase Interfaces and Its Application for Dual-Signal Chemical Sensing. *Adv. Mater.* **2019**, *31*, 1902793.
(28) Chen, G.; Liu, X.; Li, S.; Dong, M.; Jiang, D. A Droplet Energy Harvesting and Actuation System for Self-Powered Digital Microfluidics. *Lab Chip* **2018**, *18*, 1026−1034.
(29) Nie, J.; Ren, Z.; Shao, J.; Deng, C.; Xu, L.; Chen, X.; Li, M.; Wang, Z. L. Self-Powered Microfluidic Transport System Based on Triboelectric Nanogenerator and Electrowetting Technique. *ACS Nano* **2018**, *12*, 1491−1499.
(30) Zhao, X.; Zhu, G.; Fan, Y.; Li, H.; Wang, Z. L. Triboelectric Charging at the Nanostructured Solid/Liquid Interface for Area-Scalable Wave Energy Conversion and Its Use in Corrosion Protection. *ACS Nano* **2015**, *9*, 7671−7677.
(31) Zhu, H.; Tang, W.; Gao, C.; Han, Y.; Li, T.; Cao, X.; Wang, Z. L. Self-Powered Metal Surface Anti-Corrosion Protection Using Energy Harvested from Rain Drops and Wind. *Nano Energy* **2015**, *14*, 193−200.
(32) Wang, P.; Zhang, S.; Zhang, L.; Wang, L.; Xue, H.; Wang, Z. L. Non-Contact and Liquid-Liquid Interfacing Triboelectric Nanogenerator for Self-Powered Water/Liquid Level Sensing. *Nano Energy* **2020**, *72*, 104703.
(33) Wang, Z.; Yu, Y.; Wang, Y.; Lu, X.; Cheng, T.; Bao, G.; Wang, Z. L. Magnetic Flap-Type Difunctional Sensor for Detecting Pneumatic Flow and Liquid Level Based on Triboelectric Nanogenerator. *ACS Nano* **2020**, *14*, 5981−5987.
(34) Wang, Y.; Wang, Z.; Zhao, D.; Yu, X.; Cheng, T.; Bao, G.; Wang, Z. L. Flow and Level Sensing by Waveform Coupled Liquid-Solid Contact-Electrification. *Mater. Today Phys.* **2021**, *18*, 100372.
(35) Chen, J.; Guo, H.; Zheng, J.; Huang, Y.; Liu, G.; Hu, C.; Wang, Z. L. Self-Powered Triboelectric Micro Liquid/Gas Flow Sensor for Microfluidics. *ACS Nano* **2016**, *10*, 8104−8112.
(36) Lin, S.; Chen, X.; Wang, Z. L. Contact Electrification at the Liquid-Solid Interface. *Chem. Rev.* **2021**, DOI: 10.1021/acs.chemrev.1c00176.
(37) Hu, S.; Shi, Z.; Zheng, R.; Ye, W.; Gao, X.; Zhao, W.; Yang, G. Superhydrophobic Liquid-Solid Contact Triboelectric Nanogenerator as a Droplet Sensor for Biomedical Applications. *ACS Appl. Mater. Interfaces* **2020**, *12*, 40021−40030.
(38) Zhang, Q.; Jiang, C.; Li, X.; Dai, S.; Ying, Y.; Ping, J. Highly Efficient Raindrop Energy-Based Triboelectric Nanogenerator for Self-Powered Intelligent Greenhouse. *ACS Nano* **2021**, *15*, 12314−12323.

https://doi.org/10.1021/acsnano.1c08691
ACS Nano XXXX, XXX, XXX−XXX